STUDY ON KEY PARAMETERS AND FERTILIZATION PERFORMANCE OF A FLUTED-WHEEL FERTILIZER METERING DEVICE BASED ON EDEM
/
基于 EDEM 的外槽轮式排肥器关键参数和施肥性能研究

Chang WAN[1,2,3], Jiajun ZHANG[1)], Zhihui QI[1)], Zilun ZHOU[1)], Yu WANG[1)], Qingqing FAN[4)], Ling ZHOU*[1,2,3)]
[1)] College of Mechanical and Electrical Engineering, Tarim University, Alar, Xinjiang / China
[2)] Key Laboratory of Modern Agricultural Engineering of Xinjiang Uygur Autonomous Region, Alar, Xinjiang / China
[3)] Xinjiang Production and Construction Corps (XPCC) Key Laboratory of Utilization and Equipment of Special Agricultural and Forestry Products in Southern Xinjiang, Alar, Xinjiang / China
[4)] Alar Runong Modern Agricultural Technology Co., Ltd., Alar, Xinjiang / China
Correspondence author: Ling ZHOU
Tel: +8609974683855; *E-mail: zhoul-007@163.com*
DOI: https://doi.org/10.35633/inmateh-79-81

Keywords: *granular organic fertilizer, DEM calibration, fluted-wheel fertilizer metering device, fertilization uniformity, discrete element method, response surface methodology*

ABSTRACT
To address parameter optimization and fertilization uniformity of a fluted-wheel fertilizer metering device for granular organic fertilizer, a 3D-scanned fertilizer model was constructed, and an EDEM fertilization simulation model was established. The Poisson's ratio and elastic modulus of the fertilizer were determined using a texture analyzer. Drop tests were conducted to determine the coefficients of restitution between fertilizer particles and between the fertilizer and PA, PC, and PLA. Inclined-plane rolling tests were conducted to determine the rolling friction coefficients between the fertilizer and PA, PC, and PLA. A cylinder-lifting test for measuring the angle of repose, combined with EDEM simulations and a Design-Expert experimental design, was used to determine the static and rolling friction coefficients between fertilizer particles, as well as the static friction coefficients between the fertilizer and PA, PC, and PLA. By combining the discrete element method (DEM) with response surface methodology, the effects of the parameters on fertilization uniformity were ranked as follows: fluted-wheel inscribed-circle diameter > fluted-wheel lead angle > number of grooves; fertilizer-metering shaft rotational speed > fertilizer-discharge flap angle > effective working length of the fluted wheel. The optimal parameter combination was determined to be a fluted-wheel inscribed-circle diameter of 37 mm, 7 grooves, a fluted-wheel lead angle of 63°, an effective working length of the fluted wheel of 31 mm, a fertilizer-metering shaft rotational speed of 28 rpm, and a fertilizer-discharge flap angle of −1°. Soil-bin tests using 3D-printed fluted wheels with different structural parameters produced results that were generally consistent with the simulation results, providing a reference for the DEM-based optimization and design of fluted-wheel fertilizer metering devices.

摘要
针对外槽轮式排肥器施用颗粒有机肥参数优化与施肥均匀性问题，构建肥料 3D 扫描模型，建立施肥 EDEM 仿真模型。通过质构仪，获得肥料泊松比和弹性模量；通过下落试验，获得肥料与肥料、PA、PC、PLA 的碰撞恢复系数；通过斜面滚动试验，获得肥料与 PA、PC、PLA 的滚动摩擦系数；通过休止角圆筒提升试验、EDEM 仿真，结合 Design-Expert 试验设计，测定肥料与肥料静摩擦系数、滚动摩擦系数，肥料与 PA、PC、PLA 的静摩擦系数。结合离散元法（DEM）与响应面法，获得参数对施肥均匀性的影响排序分别为：槽轮内接圆直径>槽轮升角>凹槽个数；排肥轴转速>排肥舌角度>槽轮有效工作长度。最优参数组合是：槽轮内接圆直径为37mm，凹槽数量为 7，槽轮升角为 63°，槽轮有效工作长度为 31mm，排肥轴转速为 28RPM，排肥舌角度为-1°。采用 3D 打印不同结构参数槽轮，土槽试验结果与仿真基本一致，为排肥器离散元优化设计提供参考

INTRODUCTION
Discrete Element Method (DEM) can simulate fertilizer and other discontinuous agricultural materials. EDEM is a simulation software based on DEM. It comprises a pre-processor for creating and initializing discrete element models, a solver for simulation and calculation, and a post-processing module for displaying and analyzing simulation results.

Published studies have primarily focused on the calibration of discrete element parameters for fertilizers, including intrinsic parameters, basic contact parameters, and contact model parameters; parameter optimization of fertilizer metering devices; and the optimization and design of fertilizer applicators based on EDEM simulations.

The accuracy of the fertilizer particle model, the fertilizer metering device model, and the discrete element parameters forms the basis for reliable EDEM simulations. Most fertilizer particle modeling methods have used single-sphere or multi-sphere models to approximate the actual particle geometry (*Adilet et al., 2021; Xie et al., 2021; Bivainis et al., 2023; Ma et al., 2025*). Experimental designs generated using Design-Expert software, physical angle of repose tests, and discrete element simulations have been used to calibrate the contact model parameters (*Adilet et al., 2021; Xie et al., 2021; Nouh et al., 2024; Ma et al., 2025*).

EDEM was used to simulate the fertilizer discharge process, determine optimal structural and operating parameters and evaluate fertilization performance. In order to enhance the uniformity of fertilizer application, EDEM simulation of a centrifugal fertilizer spreader with two shutter holes was employed to optimize the shutter hole position (*Hwang et al., 2021*). EDEM simulations were used to conduct single-factor and orthogonal tests on the inner diameter, pitch, outlet spacing, and number of screw starts of a blocking-wheel-type screw fertilizer metering device to determine the optimal structural parameters (*Zha et al., 2021*). EDEM simulation was used to establish a simulation model of a centrifugal spreader and evaluated the lateral uniformity of a granular cylindrical organic fertilizer application (*Zinkevičienė et al., 2021*). The structural design and parameters of outer groove wheel fertilizer metering device were studied according to fertilization performance simulated using discrete element modeling (*Zeng, et al., 2020; Wang, J. F. et al., 2023*). Focusing on optimizing the spreading uniformity of a vertical spiral rotor organic fertilizer applicator, EDEM simulations were employed to investigate the effects of rotor speed and rotor inclination angle (*Ștefan et al., 2025*).

Using the coefficient of variation of fertilization uniformity as the evaluation criterion, this study proposed a DEM parameter calibration procedure and an EDEM simulation method to optimize the key parameters of a fluted-wheel fertilizer metering device for granular organic fertilizer. The DEM contact parameters between the fertilizer and three materials used in the metering device (PA, PC, and PLA) were determined. Three structural parameters (the fluted-wheel inscribed-circle diameter, number of grooves, and fluted-wheel lead angle) and three operating parameters (the effective working length of the fluted wheel, fertilizer-metering shaft rotational speed, and fertilizer-discharge flap angle) were optimized. Soil bin tests were conducted to validate the performance of the optimized parameter combination.

MATERIALS AND METHODS

Simulation model and key parameters

Model and materials of fertilizer metering device

As shown in Fig. 1(a), the fluted wheel is the core component of the fertilizer metering device, with a mounting-hole diameter of 70 mm.

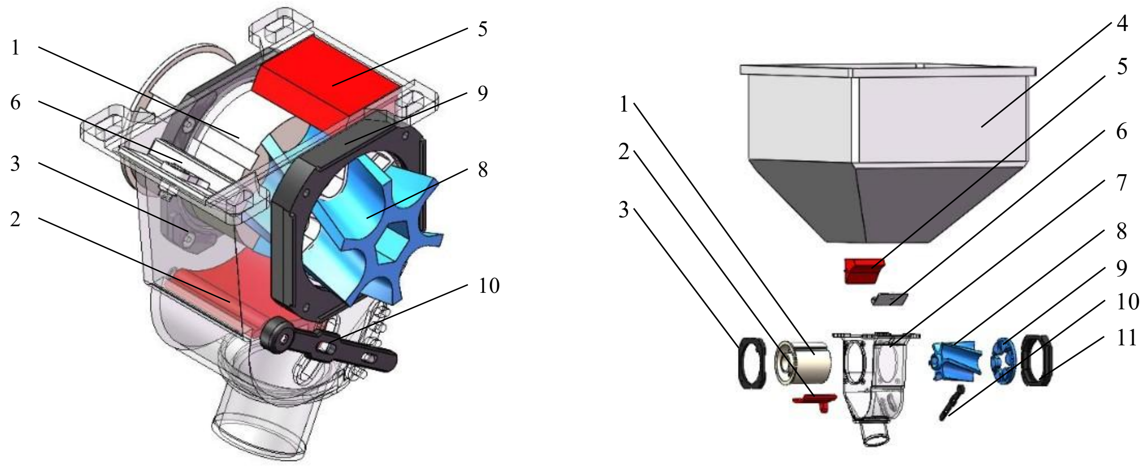

(a) Fluted-wheel fertilizer metering device (b) Exploded view of the fertilizer metering device

Fig. 1 - 3D model of the fertilizer metering device

1. blocking wheel ; 2. fertilizer discharge flap; 3. blocking-wheel fixing ring; 4. fertilizer hopper; 5. baffle; 6. brush; 7. fertilizer metering device housing; 8. fluted wheel; 9. fluted-wheel retaining ring; 10. fertilizer-discharge flap adjusting handle; 11. fluted-wheel fixing ring

Table 1 details the materials used for different components of the fertilizer metering device, including PA, PC, and PLA.

Table 1

Materials of different components of the fertilizer metering device

No.	Component	Material
1	Blocking wheel	Polyamide (PA)
2	Fertilizer metering device housing	Polycarbonate (PC)
3	Fluted wheel	Polylactic acid (PLA)
4	Fertilizer discharge flap	Polyamide (PA)
5	Baffle	Polyamide (PA)

Key parameters of fertilizer metering device

Consistent with previous literatures (*Zeng et al. 2020; Wang Y. et al. 2023*), the fertilizing amount per circle *q* and the total fertilizing amount Q of a fluted-wheel fertilizer metering device can be calculated by:

$$q = L\,\gamma\,S\,\psi\,Z \tag{1}$$

$$Q = q\,n\,t \tag{2}$$

where, L is the effective working length of fluted wheel, cm; γ is the density of fertilizer, g/cm^3; S is the cross-sectional area of a single flute, cm^2; ψ is the filling coefficient of the groove; Z is the number of grooves; n is the fertilizer-metering shaft rotational speed, RPM; t is the time of fertilizer discharge, minute.

Fig. 2 shows the fluted-wheel inscribed-circle diameter D, the number of grooves Z, and the fluted-wheel lead angle θ. Fig. 3 shows the adjustable operating parameters, namely the effective working length L of the fluted wheel, the fertilizer-metering shaft rotational speed n, and the fertilizer-discharge flap angle α. According to Eqs. (1) and (2) and previous studies (*Zeng et al., 2020; Wang Y. et al., 2023; Wang J. F. et al., 2023*), these key parameters may affect the variables involved in the equations and thereby influence fertilization uniformity.

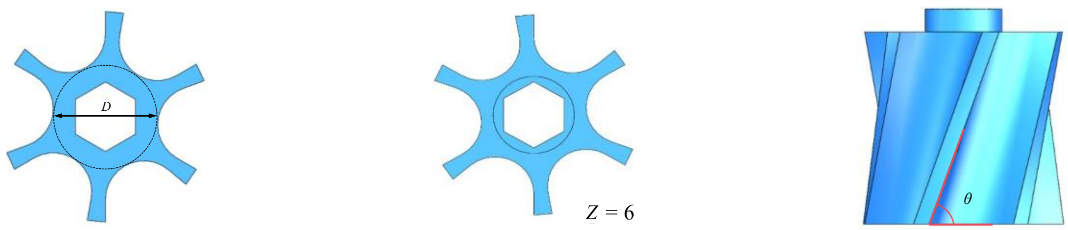

(a) fluted-wheel inscribed-circle diameter *D* (b) number of grooves *Z* (c) fluted-wheel lead angle *θ*

Fig. 2 - Structural parameters of the fluted wheel

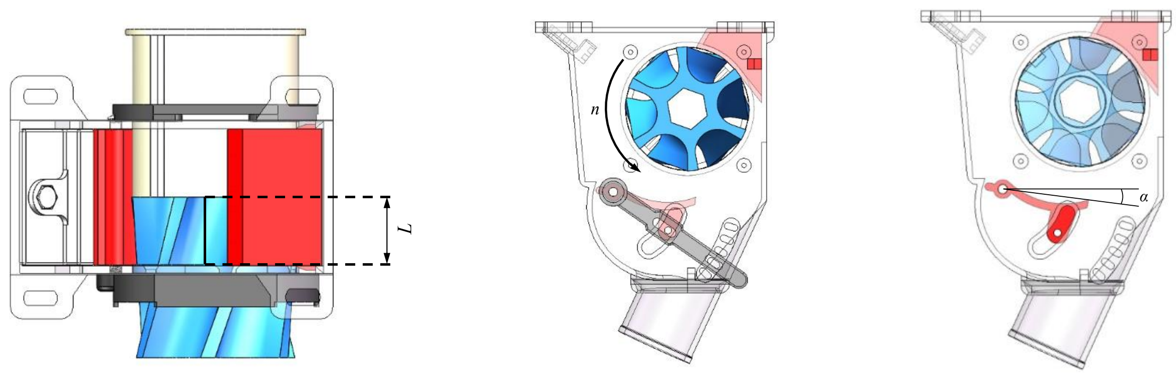

(a) effective working length *L* of the fluted wheel (b) fertilizer-metering shaft rotational speed *n* (c) fertilizer discharge flap angle *α*

Fig. 3 - Operating parameters of the fertilizer metering device

Fertilizer simulation model

This study used an amino acid organic fertilizer (China agricultural industry standard for organic fertilizer, NY525-2012), organic matter ≥ 45%, and total nutrient ($N+P_2O_5+K_2O$) ≥ 10%. The 100 fertilizer particles were randomly selected and measured using a digital display vernier caliper (DL 91200 with an accuracy of 0.01 mm) to obtain the fertilizer's average length, width, and thickness.

$$D = \sqrt[3]{LWT} \tag{3}$$

$$\phi = \frac{D}{L} \tag{4}$$

where: D is the equivalent diameter（mm）; L is the average length（mm）; W is the average width（mm）; T is the average thickness（mm）; Φ is the sphericity. The equivalent diameter D of the fertilizer was 4.29 mm, and the sphericity Φ was 97%. The proportion of particles in three intervals of large (D ≥ 5 mm), medium (4 mm < D < 5 mm), and small (D < 4 mm) were 15%, 80%, and 5%, respectively.

As shown in Fig. 4(a), the fertilizer particle was sprayed with a contrast enhancer (imaging agent), and was scanned using a 3D scanner (G5-630 with a scanning accuracy of 0.02 mm). To improve the accuracy of three-dimensional model of the fertilizer particle, the turntable was rotated approximately every 10 degrees to scan the particles, capturing surface characteristic data each time. As illustrated in Fig. 4(b), the completeness of the particle model was monitored in the software to ensure all surface feature data were acquired. After scanning, the 3D shell model of the fertilizer particle underwent noise removal and defect correction.

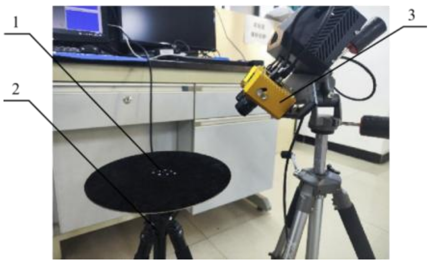

(a) fertilizer particle scanning process

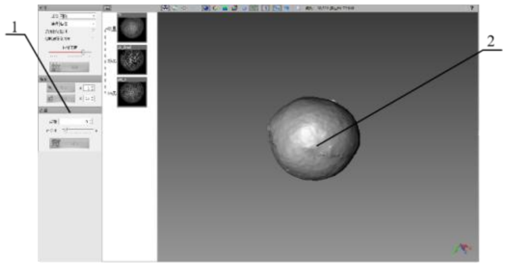

(b) interface of the scanning software

Fig. 4 - Fertilizer particle scanning and processing

(a) 1. fertilizer granule; 2. tripod turntable; 3. 3D scanner (b) 1. editing area; 2. surface model of the fertilizer granule

Figs. 5(a), 5(b), and 5(c) show three surface models obtained by 3D scanning representative large, medium, and small fertilizer granules. As shown in Figs. 5(d), 5(e), the surface models were imported into EDEM 2022 and filled with spheres to generate the corresponding DEM particle models.

(a) surface model of a large particle

(b) surface model of a medium particle

(c) surface model of a small particle

(d) sphere-filled model of a large particle

(e) sphere-filled model of a medium particle

(f) sphere-filled model of a small particle

Fig. 5 - Three-dimensional model of fertilizer particles

DEM parameter calibration method

Poisson's ratio of the fertilizer

As shown in Fig. 6, a fertilizer particle was placed at the center of the platform of a texture analyzer (TA.XTplusC, force measurement accuracy: 0.0001 N). The particle was compressed using a rigid probe at a loading rate of 5 mm/min, with an initial trigger force of 0.375 N. Loading was stopped when the fertilizer particle fractured. The transverse and longitudinal dimensions of the particle were then measured after compression.

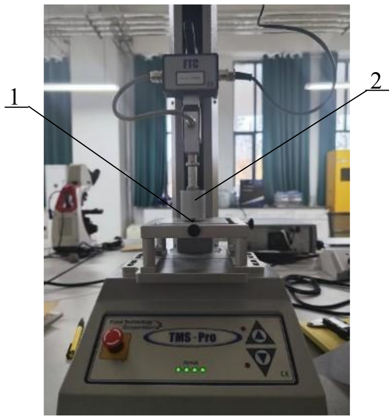

Fig. 6 - Measurement procedure using the texture analyzer
1. fertilizer particle, 2. probe

Poisson's ratio was calculated using Eq. (5). The test was repeated five times, and the mean value was used as the final result.

$$\mu = \frac{\varepsilon_T}{\varepsilon_L} = \frac{\Delta l / l}{\Delta d / d} \tag{5}$$

where: μ is the Poisson's ratio, ε_T is the transverse strain of the fertilizer particle, ε_L is the longitudinal strain of the fertilizer particle, Δl is the transverse deformation of the fertilizer particle (mm), l is the initial transverse dimension of the fertilizer particle (mm); Δd is the longitudinal deformation of the fertilizer particle (mm); d is the initial longitudinal dimension of the fertilizer particle (mm).

Elastic modulus of the fertilizer

The elastic modulus reflects a material's resistance to elastic deformation and was measured using a texture analyzer. Large fertilizer particles were selected and polished with sandpaper into cylindrical specimens. The prepared specimens were placed at the center of the loading platform and compressed using a rigid probe at a loading rate of 5 mm/min. The initial trigger force was set to 0.375 N. Fig. 7(a) shows the force–time curve, while Fig. 7(b) shows the force–time curve corresponding to the elastic deformation region. The elastic modulus was calculated using Eq. (6). The test was repeated five times, and the mean value was taken as the final result.

$$E = \frac{\sigma}{\varepsilon} = \frac{\Delta F / A}{v \cdot \Delta t / h} = \frac{h}{vA} \cdot \frac{\Delta F}{\Delta t} = \frac{kh}{vA} \tag{6}$$

where: E is the elastic modulus of the fertilizer (Pa), σ is the stress within the elastic limit, ε is the strain within the elastic limit, A is the cross-sectional area of the fertilizer specimen (mm^2), ΔF is the force increment within the elastic deformation region (N), v is the loading speed of the texture analyzer (mm/s), h is the height of the fertilizer specimen (mm), k is the slope of the elastic deformation region of the force–time curve.

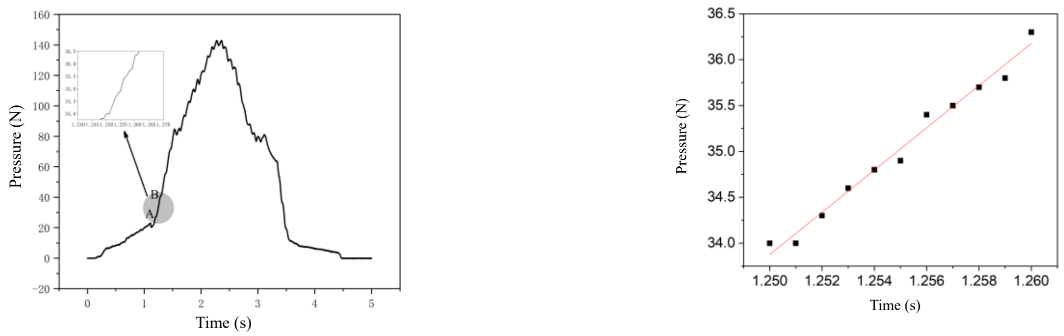

(a) force-time curve (b) linear fit of the elastic deformation region

Fig. 7 - Force–time characteristics of a fertilizer particle

Coefficient of restitution of the fertilizer

The coefficient of restitution characterizes the degree of energy loss during a collision and can be expressed as follows:

$$e = \sqrt{\frac{l_2}{l_1}} \tag{7}$$

where: l_1 is the initial drop height (m) and l_2 is the rebound height (m).

As shown in Fig. 8, the complete rebound and subsequent falling process of the fertilizer particles was recorded during the free-fall test. The rebound height of the fertilizer particles was measured, and the test was repeated five times to obtain the mean value.

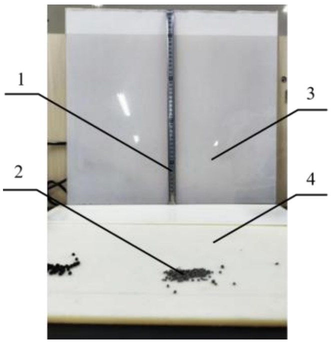

(a) coefficient of restitution test setup

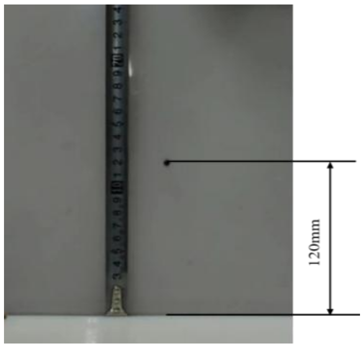

(b) slow-motion image of the rebound process

Fig. 8 - Coefficient of restitution test

1. ruler, 2. fertilizer granules, 3. background plate, 4. impact plate

Rolling friction coefficients between the fertilizer and PA, PC, and PLA

Fig. 9(a) shows the inclined-plane rolling test used in this study. Two plates made of the same material as the corresponding components of the fertilizer metering device were used. One plate was placed horizontally, while the other was inclined at 30° to the horizontal. Fertilizer granules were released from a position 100 mm above the horizontal plate and moved down the inclined plate under gravity. The rolling distance of the fertilizer granules on the horizontal plate was recorded, as shown in Table 2. The test was repeated five times, and the mean value was calculated. Fig. 9(b) shows the corresponding EDEM simulation of the fertilizer particle rolling test. As shown in Table 3, the rolling friction coefficient was varied within the range of 0.1-0.2 in the simulation tests. Each test condition was repeated five times, and the mean value was calculated.

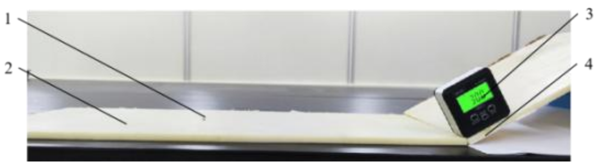

(a) inclined-plane rolling test

(b) EDEM simulation test

Fig. 9 - Calibration test for the rolling friction coefficient

1. fertilizer granule, 2. horizontal nylon plate, 3. digital inclinometer, 4. inclined nylon plate

Table 2

Results of the inclined-plane rolling test

Material pair	**Mean rolling distance [mm]**
Fertilizer - PA	212.09
Fertilizer - PC	244.09
Fertilizer - PLA	230.36

Table 3

Simulation results of the rolling test

Rolling friction coefficient / Material pair	0.10	0.12	0.14	0.16	0.18	0.20
Fertilizer - PA [mm]	357.21	276.33	232.41	195.63	152.67	136.89
Fertilizer - PC[mm]	389.47	311.96	263.25	226.34	179.35	146.23
Fertilizer - PLA[mm]	372.89	308.37	253.12	210.39	177.45	149.20

As shown in Table 4, Origin software was used to perform linear regression on the simulation data, and a fitting equation was obtained for each material pair. In the fitting equations, *y* represents the rolling distance of the fertilizer granules, and *x* represents the rolling friction coefficient. As shown in Table 5, the rolling friction coefficients between the fertilizer and PA, PC, and PLA were determined by substituting the experimentally measured rolling distances into the corresponding fitting equations.

Table 4

Fitting equations for the rolling friction coefficients

Material pair	Fitting equation
Fertilizer - PA	y=−2154.20x+548.26
Fertilizer - PC	y=−2358.49x+606.54
Fertilizer - PLA	y=−2219.91x+578.22

Table 5

Coefficient of rolling friction between fertilizer and materials

Material pair	Rolling friction coefficient
Fertilizer - PA	0.156
Fertilizer - PC	0.154
Fertilizer - PLA	0.157

Contact parameter calibration method based on the angle of repose

Due to space limitations, this section describes the calibration procedure using polyamide (PA) as an example. The calibration procedures for the other two materials, PC and PLA, were similar.

Cylinder-lifting test for the angle of repose

Fig. 10(a) shows the physical angle-of-repose test conducted using a PA cylinder. The cylinder had an inner diameter of 100 mm and a height of 200 mm. It was clamped in the chuck of a CNC milling machine, and fertilizer granules were poured into the cylinder until it was approximately 60% full. The cylinder was then lifted vertically at a speed of 1000 mm/min. After lifting, an approximately conical fertilizer pile formed on the bottom plate. Images of the fertilizer pile were imported into AutoCAD 2021, and the angle measurement tool was used to determine the angle of repose. The test was repeated five times, and the mean value was calculated. The measured angle of repose of the fertilizer granules on PA was 22.57°.

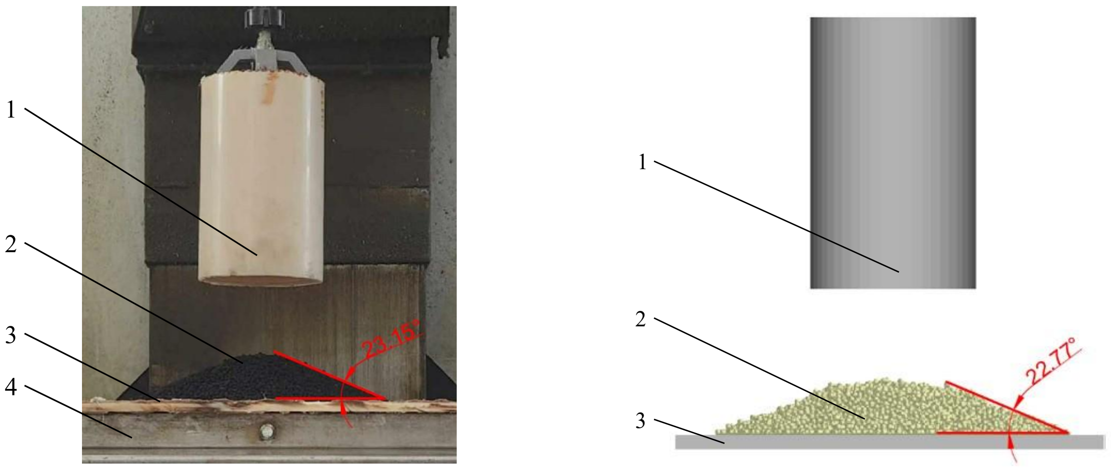

(a) physical angle of repose test using a PA cylinder (b) EDEM simulation of the angle of repose test

Fig. 10 – Angle of repose test for fertilizer granules

1. bottomless cylinder, 2. fertilizer particle pile, 3. bottom plate, 4. CNC milling machine table

Discrete element simulation of the angle of repose

As shown in Fig. 10(b), the bottomless cylinder was placed in close contact with the bottom plate. The particle factory generated fertilizer particles until the cylinder was approximately 60% full, corresponding to about 1000 g, at a generation rate of 2000 g/s. The cylinder was then lifted vertically at the same speed used in the physical test (1000 mm/min) until a stable fertilizer pile was formed. A screenshot of the final particle pile was imported into AutoCAD®, and the angle measurement tool was used to determine the angle of repose.

Plackett-Burman test

Table 6 lists the factors used in the Plackett-Burman design generated using Design-Expert 13 software. Eight parameters were selected, with each parameter assigned a high level (+1) and a low level (−1). A center point was also included in the simulation design.

Table 6

Factors and levels of the Plackett-Burman design

Parameter	Factor	Low level (-1)	High level (+1)
X_1	Poisson's ratio of the fertilizer	0.1	0.5
X_2	Shear modulus of the fertilizer	1×10^6	1×10^7
X_3	Fertilizer–fertilizer coefficient of restitution	0.1	0.7
X_4	Fertilizer–fertilizer static friction coefficient	0.1	0.9
X_5	Fertilizer–fertilizer rolling friction coefficient	0.05	0.55
X_6	Fertilizer–PA coefficient of restitution	0.1	0.7
X_7	Fertilizer–PA static friction coefficient	0.1	0.9
X_8	Fertilizer–PA rolling friction coefficient	0.05	0.55

Table 7 presents the Plackett-Burman experimental design generated using Design-Expert 13 software. EDEM simulations were then conducted to determine the angle of repose for each test combination.

Table 7

Plackett–Burman experimental design and results

No.	X_1	X_2	X_3	X_4	X_5	X_6	X_7	X_8	Angle of repose [°]
1	0.1	1×10^7	0.7	0.1	0.55	0.7	0.9	0.05	17.41
2	0.1	1×10^6	0.1	0.1	0.05	0.1	0.1	0.05	0.66
3	0.5	1×10^6	0.7	0.9	0.05	0.7	0.9	0.55	25.42
4	0.3	5.5×10^6	0.4	0.5	0.3	0.4	0.5	0.3	46.89
5	0.5	1×10^6	0.1	0.1	0.55	0.1	0.9	0.55	17.61
6	0.5	1×10^7	0.7	0.1	0.05	0.1	0.9	0.05	10.96
7	0.5	1×10^6	0.7	0.9	0.55	0.1	0.1	0.05	28.05
8	0.1	1×10^7	0.1	0.9	0.55	0.1	0.9	0.55	43.15
9	0.1	1×10^6	0.7	0.1	0.55	0.7	0.1	0.55	0.82
10	0.5	1×10^7	0.1	0.1	0.05	0.7	0.1	0.55	2.49
11	0.1	1×10^6	0.1	0.9	0.05	0.7	0.9	0.05	25.13
12	0.1	1×10^7	0.7	0.9	0.05	0.1	0.1	0.55	5.41
13	0.5	1×10^7	0.1	0.9	0.55	0.7	0.1	0.05	35.19

Table 8 shows that the fertilizer-fertilizer static friction coefficient (X_4), fertilizer-fertilizer rolling friction coefficient (X_5), and fertilizer-PA static friction coefficient (X_7) significantly affected the angle of repose of the fertilizer. The effects of the remaining factors were not significant. Therefore, these three significant factors were selected for further analysis using the steepest ascent test and the Box-Behnken design.

Table 8

Significance analysis of the Plackett-Burman design

Factor	Effect	Sum of squares	F-value	*p*-value	Significance ranking
X_1	4.52	61.38	2.05	0.23	5
X_2	2.82	23.86	0.80	0.42	7
X_3	-6.03	108.96	3.65	0.14	4
X_4	18.73	1052.81	35.22	0.01	1
X_5	12.03	433.92	14.52	0.03	2
X_6	0.10	0.03	0.0011	0.97	8

Factor	Effect	Sum of squares	F-value	*p*-value	Significance ranking
X_7	11.18	374.75	12.54	0.03	3
X_8	-3.75	42.19	1.41	0.30	6

Steepest ascent test

Table 9 presents the results of the steepest ascent test for the three significant factors. The relative error was minimized at test No. 2, indicating that the optimum region was located near this factor combination. Therefore, the factor levels corresponding to test No. 2 were selected as the center levels for the subsequent response surface design, with the adjacent lower and higher levels used as the low and high levels, respectively.

Table 9

Results of the steepest ascent test

No.	Fertilizer-fertilizer static friction coefficient (X_4)	Fertilizer-fertilizer rolling friction coefficient (X_5)	Fertilizer-PA static friction coefficient (X_7)	Angle of repose	Relative error
				[°]	[%]
1	0.1	0.1	0.05	1.08	95.21
2	0.3	0.3	0.175	25.37	12.41
3	0.5	0.5	0.3	33.22	47.19
4	0.7	0.7	0.425	38.65	71.25
5	0.9	0.9	0.55	44.56	97.43

Box-Behnken test

Table 10 presents the levels of the three significant factors used in the Box-Behnken design. A total of 15 test combinations were conducted, including three replicates at the center point.

Table 10

Box–Behnken design and test results

No.	Fertilizer-fertilizer static friction coefficient (X_4)	Fertilizer-fertilizer rolling friction coefficient (X_5)	Fertilizer-PA static friction coefficient (X_7)	Angle of repose
				[°]
1	0.1	0.05	0.3	16.75
2	0.5	0.05	0.3	25.5
3	0.1	0.3	0.3	16.1
4	0.5	0.3	0.3	42.57
5	0.1	0.175	0.1	1.72
6	0.5	0.175	0.1	7.57
7	0.1	0.175	0.5	22.37
8	0.5	0.175	0.5	41.61
9	0.3	0.05	0.1	1.5
10	0.3	0.3	0.1	5.32
11	0.3	0.05	0.5	23.97
12	0.3	0.3	0.5	34.97
13	0.3	0.175	0.3	31.78
14	0.3	0.175	0.3	30.25
15	0.3	0.175	0.3	32.64

In Table 11, the model *p*-value was less than 0.0001, indicating that the regression model was highly significant. The *p*-value for lack of fit was 0.2485, which was greater than 0.05, indicating that the lack of fit was not significant and that the model adequately fitted the experimental data. The coefficient of determination (R^2) and adjusted coefficient of determination (R^2_{adj}) were 0.9936 and 0.9821, respectively, indicating a good agreement between the predicted and experimental values. The coefficient of variation (*CV*) was 8.24%, indicating acceptable experimental reproducibility. The adequate precision value was 27.8298, which was substantially greater than 4, indicating an adequate signal-to-noise ratio.

In Eq. (8), *A* (fertilizer–fertilizer static friction coefficient), *B* (fertilizer–PA static friction coefficient), *C* (fertilizer–fertilizer rolling friction coefficient), *AB* (interaction between the fertilizer–fertilizer static friction coefficient and the fertilizer–PA static friction coefficient), B^2 (quadratic term of the fertilizer–PA static friction coefficient), and C^2 (quadratic term of the fertilizer–fertilizer rolling friction coefficient) had highly significant effects on the angle of repose θ. The interaction term *AC* (interaction between the fertilizer–fertilizer static friction coefficient and the fertilizer–fertilizer rolling friction coefficient) had a significant effect on the angle of repose. The quadratic polynomial regression equation is expressed as follows:

$$\theta = 31.56 + 7.54A + 3.90B + 13.35C + 4.43AB + 3.35AC + 1.79BC - 2.22A^2 - 4.10B^2 - 11.01C^2 \quad (8)$$

Table 11

ANOVA for the quadratic polynomial model of the Box–Behnken design

Item	Mean square	Degrees of freedom	Sum of squares	*p*-value
Model	2631.11	9	292.35	<0.0001
A	454.66	1	454.66	<0.0001
B	121.99	1	121.99	0.0018
C	1426.05	1	1426.05	<0.0001
AB	78.50	1	78.50	0.0048
AC	44.82	1	44.82	0.0149
BC	12.89	1	12.89	0.1083
A^2	18.27	1	18.27	0.0676
B^2	62.13	1	62.13	0.0078
C^2	447.95	1	447.95	<0.0001
Residual	16.90	5	3.38	
Lack of fit	13.97	3	4.66	0.2485
Pure error	2.93	2	1.47	
Total	2648.01	14		
R^2 = 0.9936, R^2_{adj} = 0.9821, *CV* = 8.24%, degree of precision = 27.8298				

Note: "P < 0.01" indicates a highly significant effect, "0.01 < P < 0.05" indicates a significant effect, and P > 0.05 indicates a nonsignificant effect.

The angle of repose measured in the physical tests was used as the target value. As shown in Fig. 11, Design-Expert 13 software was used to optimize the three parameters and generate the response surface plots.

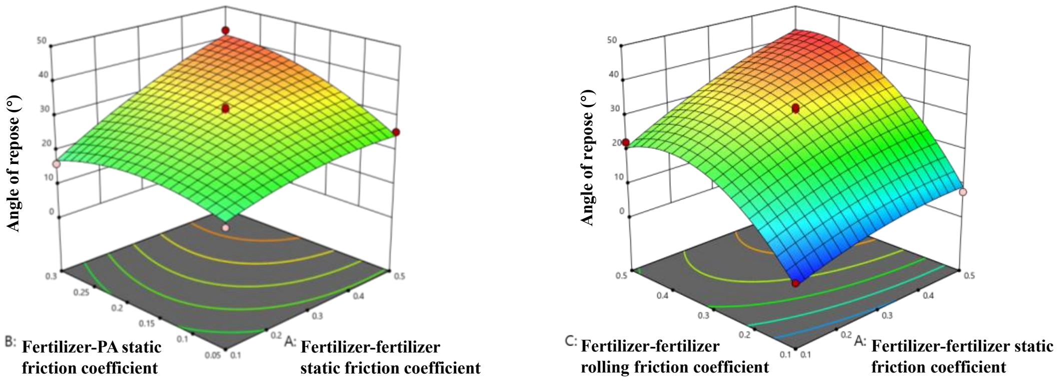

(a) fertilizer-PA static friction coefficient and fertilizer–fertilizer static friction coefficient

(b) fertilizer-fertilizer rolling friction coefficient and fertilizer-fertilizer static friction coefficient

Fig. 11 - Response surfaces of the interaction effects

The fertilizer–fertilizer static friction coefficient (*A*) was 0.402, the fertilizer–PA static friction coefficient (*B*) was 0.276, and the fertilizer–fertilizer rolling friction coefficient (*C*) was 0.177. The center values were used for the remaining parameters: the Poisson's ratio of the fertilizer was 0.3, the shear modulus of the fertilizer was 5.5×10^6 P_a, the fertilizer–fertilizer coefficient of restitution was 0.4, the fertilizer–PA coefficient of restitution was 0.4, and the fertilizer–PA rolling friction coefficient was 0.3. Three EDEM simulations of the angle of repose were conducted, yielding values of 22.10°, 22.34°, and 22.77°, respectively. The results were analyzed using a *t*-test, and $t = -1.442 < t_{0.05/2} = 2.776$, indicating that there was no significant difference between the simulated and experimentally measured angles of repose.

Contact parameter calibration results

The contact parameters between the fertilizer and the other materials (PC and PLA) were calibrated using the same procedure described above. As shown in Table 12, the calibrated fertilizer-fertilizer static and rolling friction coefficients obtained for the three material-based calibration tests were similar. Therefore, the mean fertilizer-fertilizer static friction coefficient and rolling friction coefficient were calculated as 0.413 and 0.181, respectively.

Table 12

Calibration results of fertilizer contact parameters

Contact parameter / Material pair	Fertilizer-material static friction coefficient	Fertilizer-fertilizer static friction coefficient	Fertilizer-fertilizer rolling friction coefficient
Fertilizer and PA	0.276	0.402	0.177
Fertilizer and PC	0.266	0.424	0.180
Fertilizer and PLA	0.173	0.412	0.187
Mean value		0.413	0.181

Fertilization EDEM simulation method

Coefficient of variation of fertilization uniformity

According to Chinese agricultural industry standard for technical specifications of quality evaluation for fertilizing machinery (*NY/T1003-2006, 2006*) and literature review (Bang*ura et al., 2020; Ștefan et al., 2025*), coefficient of variation of fertilization uniformity (CVFU) was calculated using Equations (9), (10), and (11).

$$\bar{m} = \frac{1}{n}\sum m_i \tag{9}$$

$$s = \sqrt{\frac{\sum (m_i - \bar{m})^2}{n-1}} \tag{10}$$

$$\sigma = \frac{s}{\bar{m}} \times 100\% \tag{11}$$

where: $\bar{m}$ is average mass of fertilizer of grid cell (g); m_i is fertilizer mass of the i-th experiment (g); n is number of experiments; s is standard deviation of n fertilizer discharge measurements; and σ is CVFU(%).

DEM parameter settings

As shown in Table 13, the fertilizer density was determined using the water displacement method, whereas the Poisson's ratio, density, and shear modulus of PA, PC, and PLA were obtained from the literature (*Zhang et al., 2019*). The remaining simulation parameters were obtained using the DEM parameter calibration procedures described above. Because the moisture content of the fertilizer granules was low, interparticle adhesion was considered negligible. The Hertz-Mindlin (no slip) model was therefore adopted as the contact model in the simulations.

Table 13

Discrete element parameters

Simulation parameter	Value	Simulation parameter	Value
Poisson's ratio of the fertilizer	0.314	Fertilizer-fertilizer coefficient of restitution	0.421
Poisson's ratio of PA	0.34	Fertilizer-PA coefficient of restitution	0.422
Poisson's ratio of PC	0.39	Fertilizer-PC coefficient of restitution	0.436
Poisson's ratio of PLA	0.43	Fertilizer-PLA coefficient of restitution	0.426
Fertilizer density (g/cm^3)	1.580	Fertilizer-fertilizer static friction coefficient	0.413
PA density (g/cm^3)	1.130	Fertilizer-PA static friction coefficient	0.276
PC density (g/cm^3)	1.200	Fertilizer-PC static friction coefficient	0.266
PLA density (g/cm^3)	1.240	Fertilizer-PLA static friction coefficient	0.173
Fertilizer elastic modulus (Pa)	9.8×10^7	Fertilizer-fertilizer rolling friction coefficient	0.181
PA shear modulus (Pa)	9.7×10^8	Fertilizer-PA rolling friction coefficient	0.156
PC shear modulus (Pa)	8.62×10^8	Fertilizer-PC rolling friction coefficient	0.154
PLA shear modulus (Pa)	1.3×10^9	Fertilizer-PLA rolling friction coefficient	0.157

EDEM simulation model

As shown in Fig. 12, Granule factory was set on fertilizer box. Total amount of fertilizer particles was 2 kg, and generation speed was 5 kg/s. Generation proportion of large, medium, and small fertilizer particles was 15%, 80%, and 5%, respectively. Forward speed of the fertilizer metering device was 1m/s. Grid bin group module was adopted, and 1000 mm was set as sampling area, divided into five areas on average (each cell size 200 mm x 1000 mm x 200 mm). Fertilizer quality of each cell was statistically analyzed. Coefficient of variation of fertilization uniformity was calculated using Equation (9), (10), and (11).

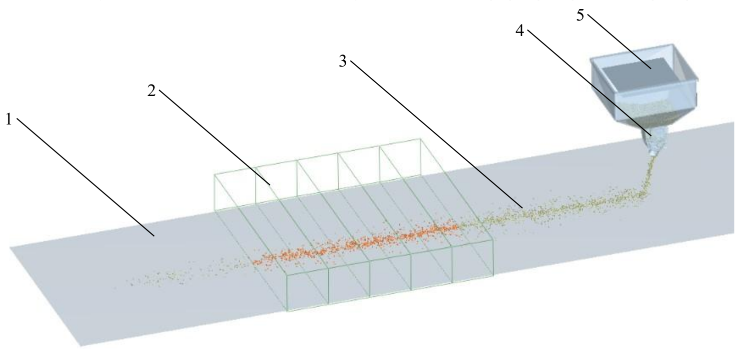

Fig. 12 - Discrete element simulation model of the fertilizer metering device

1. ground surface, 2. sampling area, 3. fertilizer particles, 4. fertilizer metering device, 5. particle factory

Soil bin test validation method

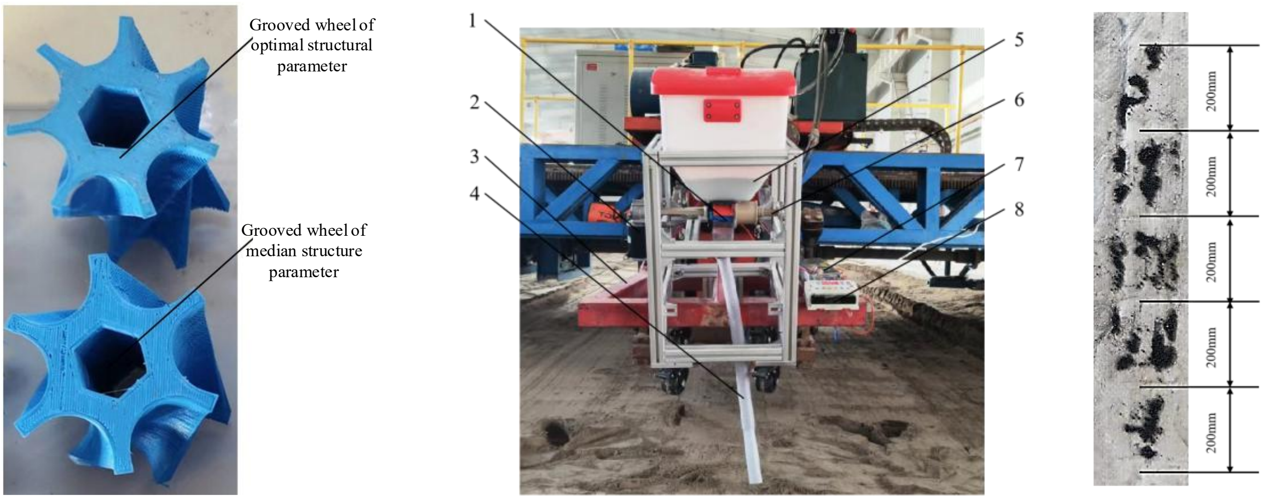

(a) 3D-printed fluted wheels (b) test apparatus (c) sampling grids

Fig. 13 - Soil bin test

1. fluted-wheel fertilizer metering device, 2. DC motor, 3. three-point hitch frame, 4. fertilizer delivery tube, 5. fertilizer hopper, 6. fertilizer-metering shaft, 7. power supply, 8. DC motor controller

Fig. 13(a) shows the two 3D-printed fluted wheels used in the test. As shown in Fig. 13(b), the test apparatus was connected to the soil-bin tractor through a three-point hitch frame. The sampling grids shown in Fig. 13(c) were consistent with those used in the simulation described above. The sampling length was 1 m and was divided into five 200 mm sections. The forward speed of the soil-bin tractor was set to 1 m/s. A DC motor drove the fluted-wheel fertilizer metering device through the fertilizer-metering shaft, and the fertilizer granules were discharged through the fertilizer delivery tube onto the sampling grids. The mass of fertilizer collected in each grid was recorded. The coefficient of variation of fertilization uniformity (CVFU) was calculated using Eqs. (9)–(11). Five sections of the fertilizer strip were randomly selected as sampling intervals.

RESULTS

EDEM simulation of the fertilization process

Operation of the fertilizer metering device

Fig. 14 shows a sectional view of the fluted-wheel fertilizer metering device, with particle velocity represented by the color scale. The structural parameters were as follows: fluted-wheel inscribed-circle diameter (D) of 38 mm, number of grooves (Z) of 6, and fluted-wheel lead angle (θ) of 65°.

The operating parameters were an effective working length of the fluted wheel (L) of 35 mm, a fertilizer-metering shaft rotational speed (n) of 35 rpm, and a fertilizer-discharge flap angle (α) of 0°.

In Fig. 14, the groove outlined in black is used as an example. As the fluted wheel rotates counterclockwise, the interval from 1.2 to 1.3 s represents the fertilizer filling stage, during which fertilizer enters the groove under gravity and the action of the fluted wheel. The interval from 1.4 to 1.7 s represents the fertilizer conveying stage, whereas the interval from 1.8 to 1.9 s represents the fertilizer discharge stage. The particle velocities in the forcing layer were markedly higher than those in the driving layer. A distinct boundary between the forcing and driving layers, together with consistent groove filling, contributed to improved fertilization uniformity.

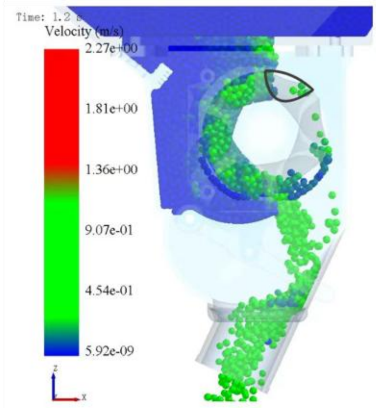

(a) 1.2s

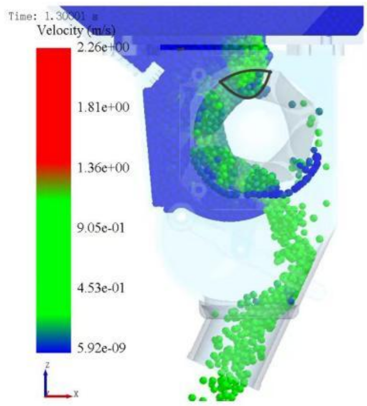

(b) 1.3s

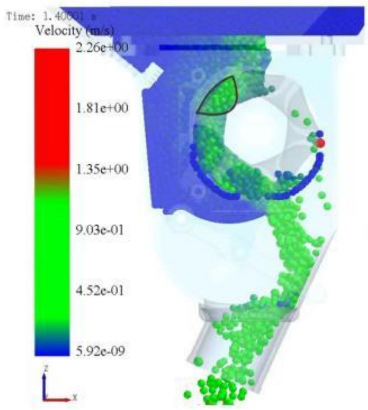

(c) 1.4s

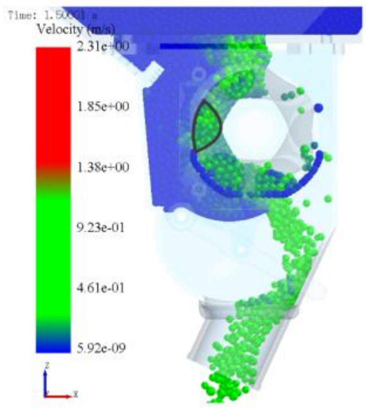

(d) 1.5s

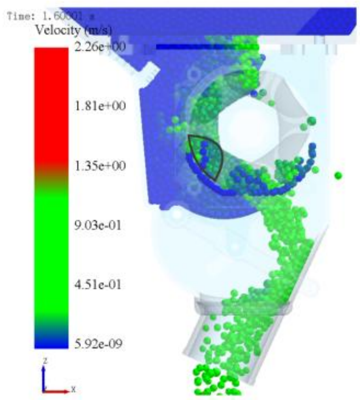

(e) 1.6s

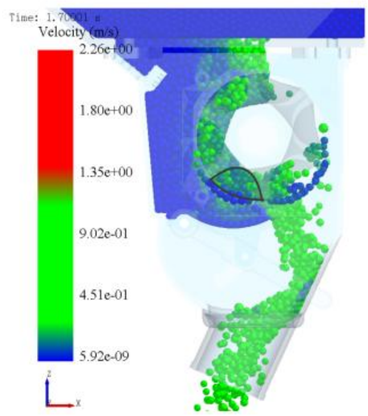

(f) 1.7s

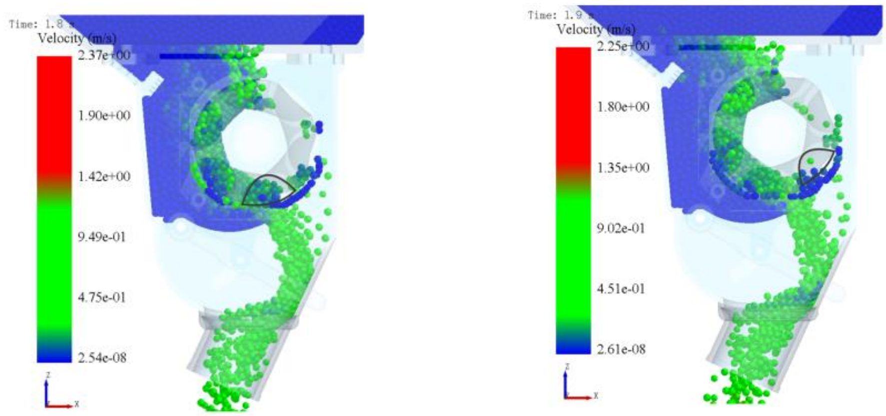

(g) 1.8s (h) 1.9s

Fig. 14 - Movement of fertilizer particles within the fertilizer metering device

Fertilizer motion during the fertilization process

Fig. 15(a) shows the velocity distribution of fertilizer particles within the fertilizer metering device. Fig. 15(b) shows the trajectory of a single fertilizer particle, and Fig. 15(c) shows the variation in particle velocity with time. Region *ab* corresponds to the particle generation stage. The particle velocity initially increases and then decreases after the particle reaches the bottom of the fertilizer hopper. Region *bc* corresponds to the fertilizer filling stage, during which the particle velocity gradually decreases from its maximum value to its minimum value. In region *cd*, the particle moves together with the fluted wheel, and its velocity remains relatively stable. Region *de* corresponds to the discharge stage from the fluted wheel, during which interaction with the fertilizer-discharge flap causes substantial fluctuations in particle velocity. Region *ef* corresponds to the final fertilizer discharge stage, in which the particle velocity increases to 2.04 m/s before impact with the ground and then decreases.

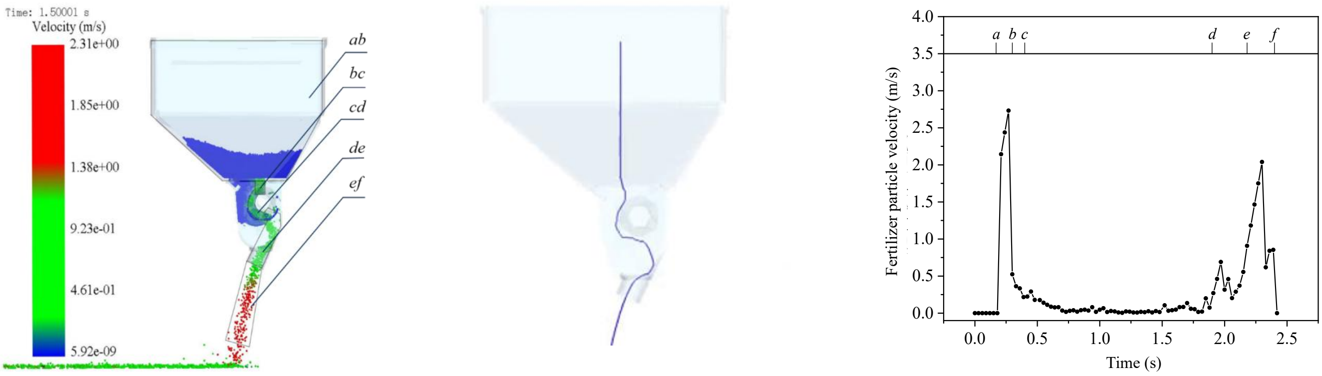

(a) fertilizer particle velocity distribution (b) trajectory of a fertilizer particle (c) variation in fertilizer particle velocity with time

Fig. 15 - Motion characteristics of fertilizer particles in the fertilizer metering device

Single-factor simulation test

Structural parameters

Fig. 16 shows that the CVFU generally decreased initially and then increased with changes in the structural parameters. The fluted-wheel inscribed-circle diameters of 34, 38, and 42 mm yielded the best results. Similarly, 5, 6, and 7 grooves produced better fertilization uniformity, while fluted-wheel lead angles of 60°, 65°, and 70° yielded the best results. Therefore, these parameter levels were selected for the subsequent multifactor tests.

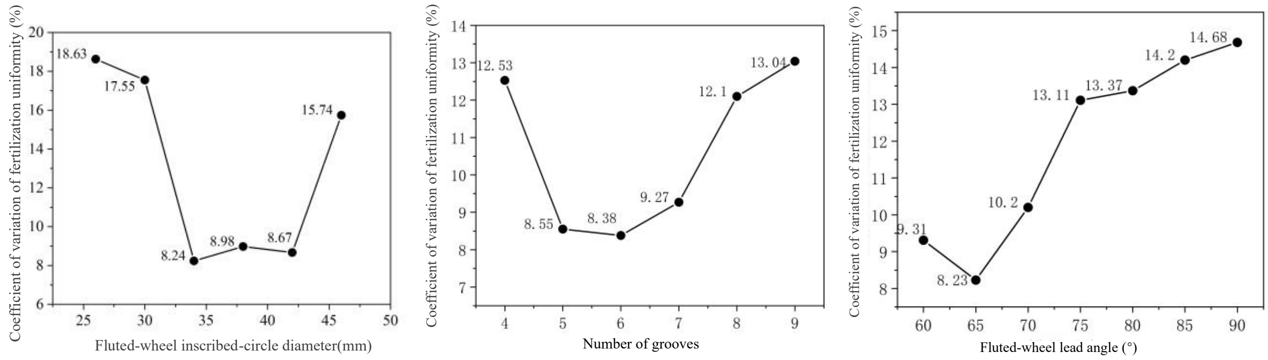

(a) fluted-wheel inscribed-circle diameter (b) number of grooves (c) fluted-wheel lead angle

Fig. 16 - Single-factor tests of the structural parameters

Operating parameters

Fig. 17 shows that the coefficient of variation of fertilization uniformity generally decreased initially and then increased as the operating parameters changed. Effective working lengths of the fluted wheel of 20, 30, and 40 mm yielded the best results. Fertilizer-metering shaft rotational speeds of 25, 35, and 45 rpm also produced better performance, while fertilizer-discharge flap angles of −5°, 0°, and 5° gave the best results. Therefore, these operating parameter levels were selected for the subsequent multifactor tests.

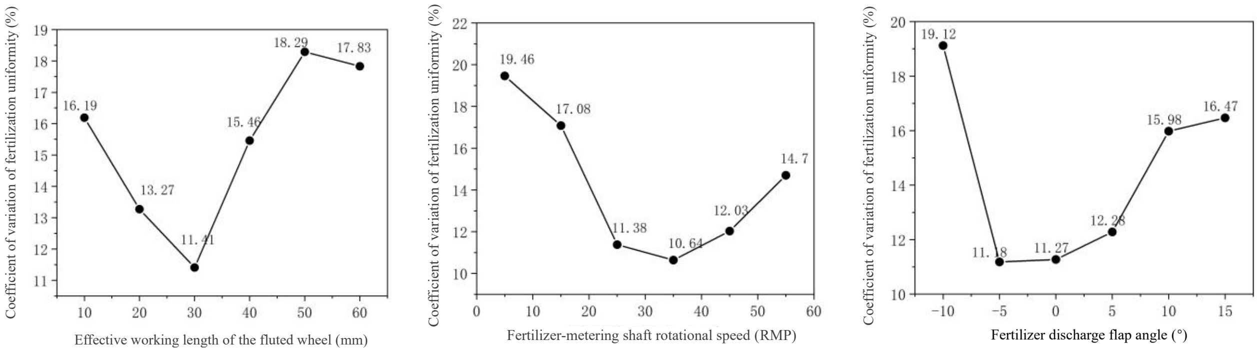

Fig. 17 - Single-factor tests of the operating parameters

Multifactor simulation test

Factor coding

Table 14

Factor levels and coding for the structural parameters

Coded level	Experimental factor		
	Fluted-wheel inscribed-circle diameter [mm]	Number of grooves	Fluted-wheel lead angle [°]
-1	34	5	60
0	38	6	65
1	42	7	70

Table 15

Factor levels and coding for the operating parameters

Coded level	Experimental factor		
	Effective working length of the fluted wheel [mm]	Fertilizer-metering shaft rotational speed [RPM]	Fertilizer discharge flap angle [°]
-1	20	25	-5
0	30	35	0
1	40	45	5

Optimization of structural parameters

The operating parameters were set to the center levels listed in Table 15. The simulation design and results for different combinations of structural parameters are presented in Table 16.

Table 16

Simulation design and results for structural parameter optimization

No.	Fluted-wheel inscribed-circle diameter	Number of grooves	Fluted wheel lead angle	Coefficient of variation of fertilization uniformity
	[mm]		[degree]	[%]
1	34	5	65	9.74
2	42	5	65	11.25
3	34	7	65	10.55
4	42	7	65	12.33
5	34	6	60	10.34
6	42	6	60	14.18
7	34	6	70	13.53
8	42	6	70	14.24
9	38	5	60	11.34
10	38	7	60	8.21
11	38	5	70	8.95
12	38	7	70	13.34
13	38	6	65	8.43
14	38	6	65	8.57
15	38	6	65	9.23
16	38	6	65	8.53
17	38	6	65	8.56

An analysis of variance (ANOVA) was performed on the regression model relating the structural parameters to the coefficient of variation of fertilization uniformity (CVFU), based on the results presented in Table 17. As shown in Table 17, the model was highly significant ($p < 0.01$). The structural parameters affected CVFU in the following order: fluted-wheel inscribed-circle diameter (*A*) > fluted-wheel lead angle (*C*) > number of grooves (*B*). The lack of fit was not significant, and the coefficient of determination (R^2) was 0.9907, indicating a good fit of the regression model.

Table 17

ANOVA of the regression model for structural parameters and CVFU

Source	Mean square	Degrees of freedom	*F* value	*p*-value	Significance
Model	73.75	9	82.74	< 0.0001	**
A	7.68	1	77.58	< 0.0001	**
B	1.24	1	12.52	0.0095	**
C	4.49	1	45.28	0.0003	**
AB	0.0182	1	0.184	0.6808	
AC	2.45	1	24.73	0.0016	**
BC	14.14	1	142.74	< 0.0001	**
A^2	25.44	1	256.85	< 0.0001	**
B^2	0.1005	1	1.01	0.3473	
C^2	16.02	1	161.74	< 0.0001	**
Lack of fit	0.2806	3	0.9064	0.5127	

*Note: ** indicates a highly significant effect ($p < 0.01$), and * indicates a significant effect ($0.01 < p < 0.05$).*

Fig. 18(a) shows that, when the fluted-wheel lead angle was fixed at 65° (center level), the coefficient of variation of fertilization uniformity first decreased and then increased as the fluted-wheel inscribed-circle diameter increased from 34 to 42 mm. When the fluted-wheel inscribed-circle diameter was fixed, the coefficient of variation of fertilization uniformity gradually increased as the number of grooves increased from 5 to 7. Fig. 18(b) shows that, when the number of grooves was fixed at 6 (center level), the coefficient of variation of fertilization uniformity first decreased and then increased as the fluted-wheel inscribed-circle diameter increased from 34 to 42 mm.

When the fluted-wheel inscribed-circle diameter was fixed, the coefficient of variation of fertilization uniformity first decreased and then increased as the fluted-wheel lead angle increased from 60° to 70°. Fig. 18(c) shows that, when the fluted-wheel inscribed-circle diameter was fixed at 38 mm (center level), the coefficient of variation of fertilization uniformity gradually decreased as the number of grooves increased from 5 to 7. When the number of grooves was fixed, the coefficient of variation of fertilization uniformity first decreased and then increased as the fluted-wheel lead angle increased from 60° to 70°.

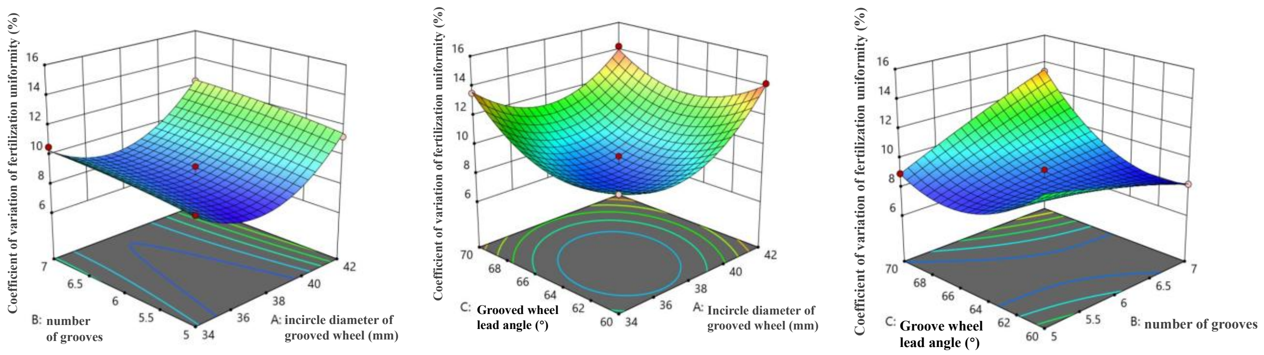

(a) fluted wheel incircle diameter and number of grooves

(b) fluted wheel incircle diameter and lead angle

(c) number of grooves and fluted wheel lead angle

Fig. 18 - Response surface diagram of the structural parameters

The regression equation relating the coefficient of variation of fertilization uniformity (*σ*) to *A*, *B*, and *C* was obtained based on the statistical analysis, as follows:

$$\begin{aligned}\sigma &= 8.66 + 0.98A + 0.3938B + 0.7487C + 0.0675AB \\ &-0.7825AC + 1.88BC + 2.46A^2 - 0.1545B^2 + 1.95C^2\end{aligned} \tag{12}$$

$$\begin{cases}\min \sigma(A,B,C) \\ A \in [34, 42] \\ B \in [5, 7] \\ C \in [60, 70]\end{cases} \tag{13}$$

Eq. (13) presents the objective function and constraints used to optimize the structural parameters of the fluted-wheel fertilizer metering device. In Eqs. (12) and (13), *σ* is the coefficient of variation of fertilization uniformity [%], *A* is the fluted-wheel inscribed-circle diameter [mm], *B* is the number of grooves, and *C* is the fluted-wheel lead angle [°]. The numerical optimization module in Design-Expert software was used to solve the optimization problem. The optimal structural parameter combination was a fluted-wheel inscribed-circle diameter of 37 mm, 7 grooves, and a fluted-wheel lead angle of 63°, corresponding to a minimum predicted coefficient of variation of fertilization uniformity of 7.95%.

Optimization of operating parameters

The structural parameters were set to the center levels listed in Table 14, and the coefficient of variation of fertilization uniformity was used as the evaluation index. The simulation design and results are presented in Table 18.

Table 18

Simulation design and results for operating parameter optimization

No.	Effective working length of the fluted wheel	Fertilizer-metering shaft rotational speed	Fertilizer-discharge flap angle	Coefficient of variation of fertilization uniformity
	[mm]	[rpm]	[°]	[%]
1	20	25	0	11.35
2	40	25	0	13.37
3	20	45	0	16.87

No.	Effective working length of the fluted wheel	Fertilizer-metering shaft rotational speed	Fertilizer-discharge flap angle	Coefficient of variation of fertilization uniformity
	[mm]	[rpm]	[°]	[%]
4	40	45	0	23.67
5	20	35	-5	13.25
6	40	35	-5	18.76
7	20	35	5	18.53
8	40	35	5	22.71
9	30	25	-5	10.76
10	30	45	-5	17.94
11	30	25	5	15.35
12	30	45	5	25.96
13	30	35	0	13.09
14	30	35	0	12.08
15	30	35	0	12.81
16	30	35	0	13.36
17	30	35	0	13.32

As shown in Table 19, an analysis of variance (ANOVA) was performed on the regression model relating the operating parameters to the coefficient of variation of fertilization uniformity (CVFU), based on the simulation results presented in Table 18. The model was highly significant ($p < 0.01$). The operating parameters affected CVFU in the following order: fertilizer-metering shaft rotational speed (*B*) > fertilizer-discharge flap angle (*C*) > effective working length of the fluted wheel (*A*). The lack of fit was not significant, and the coefficient of determination (R^2) was 0.9907, indicating a good fit of the regression model.

Table 19

ANOVA of the regression model for operating parameters and CVFU

Source	Mean square	Degree of freedom	*F*-value	*p*-value	Significance
Model	330.55	9	82.74	< 0.0001	**
A	42.83	1	96.48	< 0.0001	**
B	141.2	1	318.1	< 0.0001	**
C	59.62	1	134.32	< 0.0001	**
AB	5.71	1	12.87	0.0089	**
AC	0.4422	1	0.9962	0.3515	
BC	2.94	1	6.63	0.0368	*
A2	18.51	1	41.69	0.0003	**
B2	6.97	1	15.7	0.0054	**
C2	45.41	1	102.3	< 0.0001	**
Lack of fit	2.01	3	2.43	0.2049	

*Note: ** indicates a highly significant effect (p < 0.01), * indicates a significant effect (0.01 < p < 0.05).*

Fig. 19(a) shows that, when the fertilizer-discharge flap angle was fixed at 0° (center level), the coefficient of variation of fertilization uniformity first decreased and then increased as the effective working length of the fluted wheel increased from 20 to 40 mm. When the effective working length of the fluted wheel was fixed, the coefficient of variation of fertilization uniformity gradually increased as the fertilizer-metering shaft rotational speed increased from 25 to 45 rpm. Fig. 19(b) shows that, when the fertilizer-metering shaft rotational speed was fixed at 35 rpm (center level), the coefficient of variation of fertilization uniformity first decreased and then increased as the effective working length of the fluted wheel increased from 20 to 40 mm. When the effective working length of the fluted wheel was fixed, the coefficient of variation of fertilization uniformity first decreased and then increased as the fertilizer-discharge flap angle increased from −5° to 5°. Fig. 19(c) shows that, when the effective working length of the fluted wheel was fixed at 30 mm (center level), the coefficient of variation of fertilization uniformity gradually increased as the fertilizer-metering shaft rotational speed increased from 25 to 45 rpm. When the fertilizer-metering shaft rotational speed was fixed, the coefficient of variation of fertilization uniformity first decreased and then increased as the fertilizer-discharge flap angle increased from −5° to 5°.

The simulation results indicate that the fertilizer-metering shaft rotational speed and the effective working length of the fluted wheel affect the fertilizer filling process, which is consistent with previous findings (*Wang J. F. et al., 2023*), whereas the fertilizer-discharge flap angle affects the fertilizer discharge process.

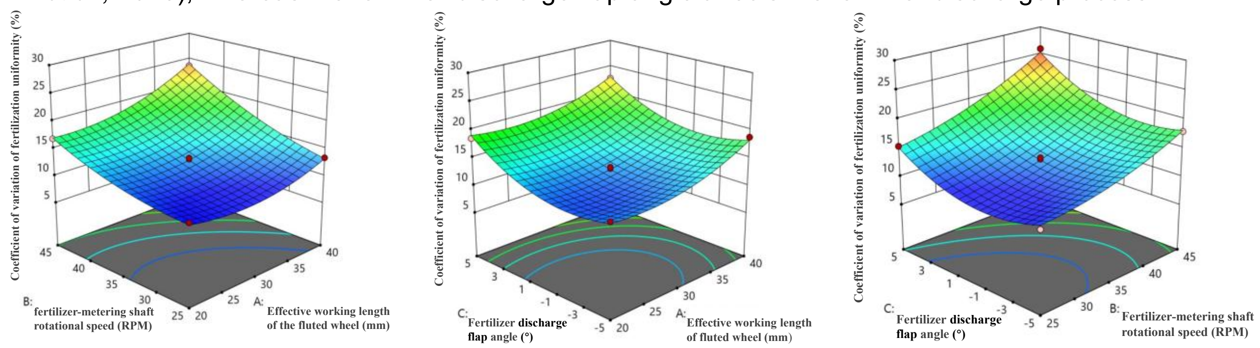

(a) effective working length of fluted wheel and fertilizer-metering shaft rotational speed

(b) effective working length of fluted wheel and fertilizer discharge flap angle

(c) fertilizer-metering shaft rotational speed and fertilizer discharge flap angle

Fig. 19 - Response surfaces of the operating parameters

The regression equation relating the coefficient of variation of fertilization uniformity (*σ*) to *A*, *B*, and *C*, derived from the statistical analysis, is given in Eq. (14). The objective function and constraints for optimization of the operating parameters of the fluted-wheel fertilizer metering device are expressed in Eq. (15).

$$\begin{aligned}\sigma &= 12.93 + 2.31A + 4.20B + 1.2C - 0.3325AB \\ &+ 0.8575BC + 2.10A^2 + 1.29B^2 + 3.28C^2\end{aligned} \quad (14)$$

$$\begin{cases}\min \sigma(A,B,C) \\ A \in [20,40] \\ B \in [25,45] \\ C \in [-5,5]\end{cases} \quad (15)$$

where *σ* is the coefficient of variation of fertilization uniformity (%); *A* is effective working length of fluted wheel [mm]; *B* is the fertilizer-metering shaft rotational speed [rpm]; and *C* is the fertilizer discharge flap angle [°]. The numerical optimization module in Design-Expert software was used to determine the optimal solution. When the effective working length of the fluted wheel was 31 mm, the fertilizer-metering shaft rotational speed was 28 rpm, and the fertilizer-discharge flap angle was −1°, the minimum predicted coefficient of variation of fertilization uniformity was 10.33%.

Soil bin test results

Optimal structural parameter

As shown in Fig. 13(a), the test of the optimal structural parameters used a 3D-printed fluted wheel with the optimal structural parameter combination obtained from the simulation: a fluted-wheel inscribed-circle diameter of 37 mm, 7 grooves, and a fluted-wheel lead angle of 63°. The center levels listed in Table 15 (an effective working length of the fluted wheel of 30 mm, a fertilizer-metering shaft rotational speed of 35 rpm, and a fertilizer-discharge flap angle of 0°) were used as the operating parameters. As shown in Table 20, the mean CVFU was 8.68%. Compared with the simulated value of 7.95%, the relative error was 12.19%. This result is generally consistent with the ranges of the coefficient of variation reported in previous studies (*Wang Y. et al., 2023*).

Table 20

Soil-bin test results for the optimal structural parameters

No.	Fertilizer mass in grid 1	Fertilizer mass in grid 2	Fertilizer mass in grid 3	Fertilizer mass in grid 4	Fertilizer mass in grid 5	Coefficient of variation of fertilization uniformity
	[g]	[g]	[g]	[g]	[g]	[%]
1	25.13	21.09	19.65	22.54	21.08	8.48
2	22.03	25.14	20.36	22.54	25.31	8.22
3	20.78	18.66	24.08	18.96	22.04	9.62
4	21.57	23.21	22.28	19.05	20.11	7.03
5	20.69	24.43	18.22	19.51	20.37	10.06
Mean value						**8.68**

Optimal operating parameters

As shown in Fig. 13(a), the test of the optimal operating parameters used a 3D-printed fluted wheel with the center-level structural parameters listed in Table 14: a fluted-wheel inscribed-circle diameter of 38 mm, 6 grooves, and a fluted-wheel lead angle of 65°. The fluted-wheel fertilizer metering device was set to the optimal operating parameters: an effective working length of the fluted wheel of 31 mm, a fertilizer-metering shaft rotational speed of 28 rpm, and a fertilizer-discharge flap angle of −1°. As shown in Table 21, the mean CVFU was 10.61%. Compared with the simulated value of 10.33%, the relative error was 2.71%.

Table 21

Soil-bin test results for the optimal operating parameters

No.	Fertilizer mass in grid 1	Fertilizer mass in grid 2	Fertilizer mass in grid 3	Fertilizer mass in grid 4	Fertilizer mass in grid 5	Coefficient of variation of fertilization uniformity
	[g]	[g]	[g]	[g]	[g]	[%]
1	25.66	19.71	18.49	22.09	24.33	12.23
2	21.05	22.95	19.65	19.2	24.63	9.49
3	22.91	21.46	25.98	20.75	19.50	10.05
4	21.06	26.85	19.25	22.32	24.58	11.67
5	22.63	24.19	18.47	23.54	20.55	9.6
Mean value						**10.61**

CONCLUSIONS

(1) This study proposed a calibration method for the discrete element simulation parameters of a granular organic fertilizer metering device. Measurements using a texture analyzer showed that the Poisson's ratio and elastic modulus of the fertilizer were 0.314 and 9.8×10^7 Pa, respectively. Coefficient of restitution tests showed that the fertilizer-fertilizer coefficient of restitution and the coefficients of restitution between the fertilizer and PA, PC, and PLA were 0.421, 0.422, 0.436, and 0.426, respectively. Rolling friction calibration tests showed that the rolling friction coefficients between the fertilizer and PA, PC, and PLA were 0.156, 0.154, and 0.157, respectively. The contact parameters between the fertilizer and the metering device materials were calibrated using a cylinder-lifting angle of repose test combined with EDEM simulations and a Design-Expert experimental design. The fertilizer-fertilizer static and rolling friction coefficients were 0.413 and 0.181, respectively, while the static friction coefficients between the fertilizer and PA, PC, and PLA were 0.276, 0.266, and 0.173, respectively.

(2) A discrete element simulation method was proposed to optimize the key parameters of a fluted-wheel fertilizer metering device. The coefficient of variation of fertilization uniformity was used as the evaluation index of fertilization performance. By combining the discrete element method (DEM) with response surface methodology, the effects of the parameters on fertilization uniformity were ranked as follows: fluted-wheel inscribed-circle diameter > fluted-wheel lead angle > number of grooves; fertilizer-metering shaft rotational speed > fertilizer-discharge flap angle > effective working length of the fluted wheel. Fluted wheels with the optimal and center-level structural parameters were fabricated by 3D printing and tested in a soil bin to validate the simulation results. The simulation and soil-bin tests identified two optimal parameter combinations: (1) a fluted-wheel inscribed-circle diameter of 37 mm, 7 grooves, and a fluted-wheel lead angle of 63°; and (2) an effective working length of the fluted wheel of 31 mm, a fertilizer-metering shaft rotational speed of 28 rpm, and a fertilizer-discharge flap angle of −1°.

ACKNOWLEDGEMENT

This paper was supported by the Xinjiang Provincial Key Project Fund (Ling ZHOU, No. 2025AB005), the Key Core Technology Research Project of Agriculture in Xinjiang Production and Construction Corps, China (Ling ZHOU, research on resource utilization model of livestock and poultry manure, development & integrated demonstration of production processes, grant number: [2023] No. 11 by Agriculture Bureau of Xinjiang Production and Construction Corps), the Project of the Innovation and Development Support Plan for Key Industries in Southern Xinjiang of China (Chang WAN, No. 2020DB003-04), the postgraduate research innovation project of Tarim University (Zilun ZHOU, No. TDGRI202347).

REFERENCES

[1] Adilet, S., Zhao, J., Sayakhat, N., Chen, J., Nikolay, Z., Bu, L., Sugirbayeva, Z., Hu, G., Marat, M., & Wang, Z. (2021). Calibration strategy to determine the interaction properties of fertilizer particles using two laboratory tests and DEM. *Agriculture*, 11(7), 592. https://doi.org/10.3390/agriculture11070592

[2] Bangura, K., Gong, H., Deng, R., Tao, M., Liu, C., Cai, Y., Liao, K. Liu, J. & Qi L. (2020). Simulation analysis of fertilizer discharge process using the Discrete Element Method (DEM). *PLoS ONE*, 15(7): e0235872. https://doi.org/10.1371/journal.pone.0235872

[3] Bivainis, V., Jotautienė, E., Lekavičienė, K., Mieldažys, R., & Juodišius, G. (2023). Theoretical and experimental verification of organic granular fertilizer spreading. *Agriculture*, 13(6), 1135. https://doi.org/10.3390/agriculture13061135

[4] Hwang, S.-J., & Nam J.-S. (2021). DEM simulation model to optimise shutter hole position of a centrifugal fertiliser distributor for precise application. *Biosystems Engineering*, 204, 326-345. https://doi.org/10.1016/j.biosystemseng.2021.02.004

[5] Ma, X., You, Y., Yang, D., Wang, D. & Hu,i Y. (2025). Discrete element parameter calibration of compound fertilizer used in Camellia oleifera planting areas. *Journal of Mechanical Science & Technology*, 39(10), 5997–6009. https://doi.org/10.1007/s12206-025-0830-0

[6] Nouh, S. A., Kushaari, K. Z., Keong, L. K., & Samsuri, S. (2024). Material characterization and inter/intra-particle validation for DEM simulation of urea coating process. *Particuology*, 88, 32-48. https://doi.org/10.1016/j.partic.2023.09.010

[7] Ștefan, V., Popa, L., Harabagiu, A., Ciupercă, R., Zaica, A., & Vișan, A. (2025). Optimization of organic fertilizer distribution using EDEM simulation analysis. *INMATEH - Agricultural Engineering*, 76(2), 1217-1230. https://doi.org/10.35633/inmateh-76-102

[8] Wang, J. F., Wang, R. D., Ju, J. Y., Song, Y. L., Fu, Z. D., Lin, T. H., Chen, G. Q., Jiang, R., & Wang, Z. (2023). Study on the influence of grooved-wheel operating parameters on fertilizer emission performance and parameter optimization. *Agronomy*, 13(11), 2779. https://doi.org/10.3390/agronomy13112779

[9] Wang, Y., Tan, Y. P., Wei, S. L., Liao, M.M.，Zang, Y. & Zeng, S. (2023). Design and experimental study of the fertilizer applicator with vertical spiral fluted roller. *International Journal of Agricultural and Biological Engineering*, 17(3), 102–112. https://doi.org/10.25165/j.ijabe.20231605.7555

[10] Xie, C., Yang, J., Wang, B., Zhuo, P., Li, C., & Wang, L. (2021). Parameter calibration for the discrete element simulation model of commercial organic fertilizer. *International Agrophysics*, 35(01), 107-117. https://doi.org/10.31545/intagr/134141

[11] Zeng, S., Tan, Y. P., Wang, Y., Luo, X. W., Yao, L. M., Huang, D. P., & Mo, Z. W.（2020）Structural design and parameter determination for fluted-roller fertilizer applicator. *International Journal of Agricultural and Biological Engineering*, 13(2): 101–110. https://doi.org/10.25165/j.ijabe.20201302.4999

[12] Zha, X., Zhang, G., Han, Y., Salem, A. E., Fu, J., & Zhou, Y. (2021). Structural optimization and performance evaluation of blocking wheel-type screw fertilizer metering device. *Agriculture*, 11(3), 248. https://doi.org/10.3390/agriculture11030248

[13] Zhang, Y. L., Li, P., Shi, L., & Zhang, W. D. (2019). *Practical engineering plastics handbook (实用工程塑料手册)*, Second Edition, China Machine Press, Beijing / China, ISBN: 9787111620792.

[14] Zinkevičienė, R., Jotautienė, E., Juostas, A., Comparetti, A., & Vaiciukevičius, E. (2021). Simulation of granular organic fertilizer application by centrifugal spreader. *Agronomy*, 11(2), 247. https://doi.org/10.3390/agronomy11020247